

Evaluation of alpha particle emission rate due to the p-11B fusion reaction in the Large Helical Device

K. Ogawa,^{a,b*} M. Isobe,^{a,b} H. Nuga,^a R. Seki,^{a,b} S. Ohdachi,^{a,c} and M. Osakabe^{a,b}

^a*National Institute for Fusion Science, National Institutes of Natural Sciences, Toki, 509-5292, Japan*

^b*The Graduate University for Advanced Studies, SOKENDAI, Toki, 509-5292, Japan*

^c*University of Tokyo, 113-8654, Japan*

*E-mail: ogawa.kunihiro@nifs.ac.jp

TEL: +81-572-58-2229

FAX: +81-572-58-2624

Total pages: 20

Total number of figures: 9

Evaluation of alpha particle emission rate due to the p-¹¹B fusion reaction in the Large Helical Device

K. Ogawa, M. Isobe, H. Nuga, R. Seki, S. Ohdachi, and M. Osakabe

Abstract

A numerical study of the alpha particle emission rate due to the p-¹¹B fusion reaction based on the respectively obtained Large Helical Device (LHD) plasma parameters in an experiment is performed. First, the total alpha particle emission rate is estimated by employing the beam ion distribution calculation code FIT3D and the fusion reaction rate calculation code FBURN based on the classic confinement of beam ions. Then, the calculation is performed using hydrogen-beam-heated hydrogen plasma parameters and the radial boron density profile obtained from boron drop discharge. The result shows that the total alpha particle emission rate reaches approximately 10^{14} s^{-1} . Then, based on the radial profile of the alpha particle emission calculated by the FBURN code, the distribution of the first orbit loss of 5.727 MeV alpha particles created by the p-¹¹B reaction on the vacuum vessel and the divertor plate is calculated by the collisionless Lorentz orbit code LORBIT. Although most of the alpha particles are lost to the divertor plate, some of the alpha particles are lost on the vacuum vessel. Finally, a feasibility study of alpha particle detection by the existing manipulators and fast ion loss detector position is performed. The number of particles as a function of position shows that a substantial number of alpha particles can be detected. Alpha particles with a pitch angle of ~ 130 degrees can reach manipulator positions. In contrast, particles with pitch angles of ~ 50 degrees and ~ 110 degrees can reach the fast ion loss detector position. The calculation shows that measurement of

alpha particles due to $p\text{-}^{11}\text{B}$ is thought to be possible using charged particle detectors.

Keywords: word; Large Helical Device, aneutronic fusion, $p\text{-}^{11}\text{B}$ reaction, alpha particle emission

I. INTRODUCTION

Research on the realization of a first-generation fusion reactor has been intensively performed based on deuterium-tritium reactions. As a near-future application, self-heating of plasma using the deuterium-tritium fusion-born alpha particle has been demonstrated in ITER.¹ In a first-generation reactor, a deuterium-tritium fusion-born 14 MeV neutron is utilized for power generation.² In addition, the study of aneutronic fusion, a fusion reaction that emits no neutron, has recently regained the spotlight. One of the most practical aneutronic fusion reactors is based on the $p\text{-}^{11}\text{B}$ reaction ($^{11}\text{B}(p,\alpha)2\alpha$).³ The fusion cross section of $p\text{-}^{11}\text{B}$ has a local maximum around the incident particle energy of 135 keV,^{4, 5} as shown in Fig. 1. This local maximum corresponds to the energy level of the compound nucleus ^{12}C , which decays to three alpha particles via $\alpha + ^8\text{Be}$.⁶ The potential of the $p\text{-}^{11}\text{B}$ reaction for thermonuclear fusion reactors was investigated in magnetic confinement devices^{7, 8} and in particular the Large Helical Device (LHD)-type magnetic field configuration combined with an ion cyclotron range of frequency heating.⁹ It was reported that the effective proton temperature needed for ignition conditions is on approximately 300 keV, which is very difficult to achieve with the current technology. More realistically, a relatively high $p\text{-}^{11}\text{B}$ reaction rate can be achieved in boron-doped plasma using a high-energy hydrogen beam. For the feasibility of a beam fusion reactor, estimation of the $p\text{-}^{11}\text{B}$ reaction rate in existing plasma is important. LHD is equipped with negative-ion-based intensive

neutral beam (NB) injectors,¹⁰ whose acceleration energy is approximately 180 keV, and with an impurity powder dropper injecting boron grains into a plasma.¹¹ Therefore, a significant p-¹¹B fusion reaction rate could be achieved in LHD by utilizing existing equipment. In this paper, the estimation of the p-¹¹B fusion reaction rate in an LHD is reported for studying the spacial/energy distribution of alpha particles produced by the p-¹¹B fusion reactions in the magnetic confinement fusion machine.

II. SETUP FOR CALCULATION

Figure 2 shows the calculation scheme adopted in this study. The alpha particle emission rate due to p-¹¹B fusion reactions is calculated using the FIT3D code^{12, 13} and the FBURN code¹⁴ in a hydrogen-beam-heated hydrogen plasma with a boron drop. The radial profiles of electron temperature and density are measured in an experiment. The ion temperature is assumed to be the same as the electron temperature. Three-dimensional magnetohydrodynamic equilibrium is reconstructed by VMEC2000¹⁵. Here, the radial profile of boron density is given from the experimental observation. The FIT3D code consists of three parts: NB deposition calculation, beam ion orbit following calculation, and steady-state analytic Fokker Planck calculation. In the deposition calculation, attenuation of NBs due to boron is newly implemented according to the stopping coefficient of the beam¹⁶. The orbit calculation is performed to estimate the prompt loss and orbital effect in the short time of 20 μ s. Then, the radial beam ion distribution is obtained. The FBURN code calculates the alpha particle emission rate using the beam ion distribution obtained by the FIT3D code based on the classical confinement of beam ions, where beam ions slow down without moving radially. Finally, the alpha particle loss point on the vacuum vessel/the divertor plate and the feasibility study of detecting alpha particles are estimated by the collisionless Lorentz

orbit code LORBIT.¹⁷ The LORBIT code solves the equation of motion of a charged particle in the static magnetic field. Here, an electric potential is not included because the electric potential formed inside the plasma is negligibly smaller (typically several keV)¹⁸ than the alpha particle energy (MeV range). An alpha particle is judged to be detected when the distance between the alpha particle and the detector becomes less than the Larmor radius.

III. THE ALPHA PARTICLE EMISSION RATE CALCULATION IN HYDROGEN PLASMA DISCHARGE

In this calculation, we used the respectively obtained plasma parameters in LHD experiments. The radial profile of the boron density is obtained in the so-called boron dropper discharge #169626 (Fig. 3 top). Here, boron grain is dropped from the upper side of a plasma from $t = 4$ s to the end of discharge. The plasma is initiated by electron cyclotron heating (ECH), and then hydrogen beams NB1, NB2 and NB3 are injected. Here, NB4 is injected for charge exchange recombination spectroscopy (CXRS) diagnostics¹⁹ to measure the boron density profile. The injection energies of NB1, NB2, NB3, and NB4 are ~ 140 keV, ~ 140 keV, ~ 135 keV, and ~ 42 keV, respectively. The line-averaged electron density measured by the far-infrared interferometer²⁰ is almost constant at approximately $2 \times 10^{19} \text{ m}^{-3}$ during discharge. The central electron temperature (T_{e0}) measured by Thomson scattering diagnostics²¹ is approximately 3 keV except at the initial and end phases of the discharge. The time evolution of the radial profile of the boron density by the CXRS diagnostics is shown at the bottom of Fig. 3 top. Here, we evaluate the absolute value of boron density by relative calibration of C^{6+} density using charge exchange cross sections of C^{6+} and B^5 .²² The boron density gradually increases with time and is almost saturated at $t = 7$ s. The radial profile of the

boron density at $t = 8.37$ s shows that a relatively hollow boron density profile is formed (Fig. 3 bottom). The peak boron density is located in the outer region of plasma, where the normalized effective minor radius (r_{eff}/a_{99}) is approximately 0.7 and the boron density is $\sim 7 \times 10^{16} \text{ m}^{-3}$. We used this boron density profile with the assumption that it does not change over time in this calculation for evaluating the maximum expected alpha particle emission rate.

The plasma parameter of a hydrogen-beam-heated hydrogen plasma obtained from the typical hydrogen discharge #168156 is used for alpha particle emission calculation (Fig. 4 top). Relatively high-performance discharge, i.e., intense plasma heating compared with boron drop discharge #169626, is chosen for obtaining an intense alpha particle emission rate because of the longer slowing down time of energetic proton due to the relatively high electron temperature. The plasma is sustained by ECH and the hydrogen beams NB1, NB2, NB3 NB4, and NB5. The injection energies of NB1, NB2, NB3, NB4, and NB5 are ~ 180 keV, ~ 165 keV, ~ 164 keV, ~ 45 keV, and ~ 46 keV, respectively. Here, the contribution of energetic proton injected by NB4 and NB5 to the alpha particle emission rate is thought to be small compared to NB1, NB2, and NB3 because the injection energy of NB4 and NB5 is below the reactivity peak. The line-averaged electron density is approximately $2 \times 10^{19} \text{ m}^{-3}$. The central electron temperature is approximately 6 keV due to the relatively high-power NB injection and the overlap of ECH. Figure 4 bottom shows the time evolution of the alpha particle emissivity profile and the alpha particle emission rate calculated by the FBURN code. The alpha particle emissivity has a peak in the plasma core region around r_{eff}/a_{99} of 0.3 because of the relatively long slowing down time of beam ions in the central region of plasma due to the relatively high electron temperature. The calculation results show that the peak alpha particle emissivity is slightly less than $6 \times 10^{12} \text{ m}^{-3} \text{ s}^{-1}$.

The alpha particle emission rate increases rapidly due to the accumulation of energetic protons and then saturated within 200 ms. From t of 4.7 s, the alpha particle emission rate slightly decreases because of the shorter slowing down the time of energetic proton due to the electron temperature decrease and the plasma density increase. Finally, the alpha particle emission rate rapidly decreases due to the NB stop. A significant amount of alpha particle emission ($1.5 \times 10^{14} \text{ s}^{-1}$) is expected by this estimation.

IV. DISCUSSION FOR ALPHA PARTICLE MEASUREMENT

A feasibility study of the measurement of alpha particles is performed by the LORBIT code. Figure 5 shows the typical Poincaré plot of co-going transit alpha particles with an energy of 5.87 MeV and a pitch angle of 30 degrees. The magnetic field in a vacuum is used with a toroidal magnetic field strength of 2.75 T and a magnetic axis position of 3.60 m. The toroidal magnetic field is directed counterclockwise from the top view. Therefore, the gradient of the magnetic field drift is directed upward. The starting point of the alpha particle is set to (R, Z) of (3.7 m, -0.5 m) in the vertically elongated poloidal cross section. The Larmor radius of the alpha particle is ~ 6 cm, which corresponds to 10% of the plasma minor radius. The deviation of an orbit from the flux surface is substantially large due to the high energy of an alpha particle. In the vertically elongated poloidal cross section, an alpha particle passes through the plasma center at the inboard side, whereas the particle extends beyond the last closed flux surface and near the vacuum vessel at the outboard side. In a horizontally elongated poloidal cross section, an alpha particle passes through the plasma center at the inboard side, whereas the particle almost follows the last closed flux surface at the outboard side.

Loss points of an alpha particle on the vacuum vessel and the divertor plate are calculated by the LORBIT code. In this calculation, the number of particles is set to 10^7 . Here, the number of particles 10^7 is chosen because the trend of toroidal/poloidal loss profile shown in Fig. 6c is almost unchanged from the result obtained with 10^6 particles. Therefore, the basic trend of the loss pattern is thought to be unchanged when the number of particles increases. It is worth noting that the calculation accuracy improves with the increase of the number of particles. The number of particles needs to be increased when detector response is included to evaluate the detection rate sensitivity in the future work. Figure 6a, b shows the three-dimensional plot of loss points (blue) and the shape of the vacuum vessel/the divertor plate (red). The loss points of alpha particles are concentrated on one side of the vacuum vessel, as obtained in the 1 MeV triton loss calculation.²³ The toroidal/poloidal distribution of alpha particle loss is plotted in Fig. 6c. Herein, the size of the toroidal/poloidal grid is set to be two degrees. The alpha particle loss mainly accumulates on the upper side of the vacuum vessel due to the gradient magnetic field drift. The stripe-like structure that appears on the upper side of the torus corresponds to the divertor plate. Although most of the alpha particles are lost on the divertor region, some alpha particles are lost on the vacuum vessel. Measurement of alpha particles is thought to be possible if a newly charged particle detector is mounted on the upper side of the vacuum vessel.

For the feasibility of alpha particle detection using the existing components without breaking the main vacuum, the number of particles that reach the existing manipulator and the fast ion loss detector positions are evaluated by the LORBIT code. Here, the manipulator installed at the lower side of the plasma^{24,25} and a fast ion loss detector²⁶ are considered. Figure 7a shows the manipulator installed on the 4.5 L port, whereas Fig. 7b shows the manipulator installed on the 10.5 L port. The blue and red

circles shown in Figs. 7a and 7b indicate the candidate manipulator head position considered in this calculation. Note that the point above the divertor leg is for reference because the manipulator cannot go through the divertor plate due to the heat load issue in an NB-heated plasma discharge. Figure 7c shows the fast ion loss detector position when the detector head is located in the innermost position. The number of alpha particles reached as a function of the detector positions and the divertor leg position is shown in Fig. 8. For the 4.5 L port manipulator, the number of alpha particles rapidly decreases due to the Z position, and the number of alpha particles becomes 0 at a Z of -1.7 m. The alpha particle detection rate is $\sim 1000/10^7 = 10^{-4}$ without going through the divertor leg. For the 10.5 L port manipulator, the number of alpha particles gradually decreases due to the Z position, and the number of alpha particles becomes 0 at a Z of -1.7 m. The alpha particle detection rate is $\sim 2500/10^7 = 2.5 \times 10^{-4}$ without going through the divertor leg, which is almost 2.5 times higher than the rate for the 4.5 L position. For the FILD, the number of alpha particles has no monotonous structure. The number of alpha particles reaching the FILD is larger than the number of alpha particles for the manipulator position. The significant increase in alpha particles at an R of 5.2 m corresponds to the alpha particles going along the divertor leg. Although a significant number of alpha particles come to the FILD in this position, the measurement of alpha particles is thought to be impossible because of the considerable heat load from bulk plasma. The alpha particle detection rate is approximately 10^{-3} . The pitch angle distributions of the alpha particle at Z of -1.39 m for the 4.5 L port manipulator, Z of -1.42 m for the 10.5 L manipulator, and an R of 4.86 m for the FILD are shown in Fig. 9. Here, the innermost position without going through the divertor led is chosen for the manipulators, and the innermost position is chosen for the FILD. For the 4.5 L port manipulator, alpha particles with a pitch angle of 120 degrees to 150 degrees can be

detected (Fig. 9a). For the 10.5 L port manipulator, alpha particles with a pitch angle of 100 degrees to 140 degrees can be detected (Fig. 9b). A charged particle detector such as a proton detector²⁷ or a diamond detector²⁸ mounted on the manipulator is a candidate for detecting alpha particles. The expected number of particles will be estimated in the detailed design phase by considering the sizes of the aperture and the detector. The alpha particles barely counter the passing transit orbit. For FILD, an alpha particle with pitch angles of 40 degrees to 50 degrees and 100 degrees to 140 degrees can be detected (Fig. 9c). Barely co-going transit, transition, and barely counter passing transit alpha particles can reach the FILD position. However, due to the limitation of the FILD structure, only barely co-going transit alpha particles can be detected.

V. SUMMARY

The alpha particle emission rate due to p-¹¹B reactions is estimated in hydrogen beam-heated hydrogen plasma with boron drops. The calculation is performed using the beam ion distribution calculation code FIT3D and alpha particle emission calculations based on the classic confinement of beam ions using the FBURN code. The estimated alpha particle emission rate is 10^{14} s^{-1} using the plasma parameters obtained from an LHD plasma experiment. The loss pattern of 5.87 MeV alpha particles on the vacuum vessel and the divertor plate is calculated by collisionless Lorentz orbit calculation LORBIT code. The loss point of alpha particles accumulates at the top and one side of the vacuum vessel due to the gradient of the magnetic field drift. A feasibility study of alpha particle measurement using existing manipulators or the FILD is performed. A substantial number of alpha particles reach the manipulator located outside of the divertor legs. Alpha particle detection is thought to be possible by using the charged particle detector mounted on the manipulator or the FILD. A study of p-¹¹B fusion in

LHD has a potential not only for understanding aneutronic fusion but also for the non-fusion applications, e.g., irradiation of electric circuit working in high-irradiation conditions²⁹ or cell system³⁰, as the relatively intense volumetric source of the alpha particles.

REFERENCES

- Ref1. K. IKEDA et al., “Progress in the ITER Physics Basis”, *Nucl. Fusion* **47** E01 (2007).
- Ref2. F. L. RIBE, “Fusion reactor systems”, *Rev. Mod. Phys.* **47** 7 (1975).
- Ref3. R. FELDBACHER and M. Heindler, “Nuclear-physics aspects of controlled thermonuclear fusion: Analysis of promising fuels and gamma-ray diagnostics of hot plasma”, *Nucl. Instrum. Meth. Phys. Res. A* **271** 55 (1988).
- Ref4. W. M. NEVINS AND R. SWAIN, “The thermonuclear fusion rate coefficient for p-11B reactions”, *Nucl. Fusion* **40** 865 (2000)19
- Ref5. F. A. GESER AND M. VALENTE, “A theoretical model for the cross section of the proton-boron fusion nuclear reaction”, *Radiat. Phys. Chem.* **167** 108224 (2020).
- Ref6. D. C. MOREAU, “Potentiality of the proton-boron fuel for controlled thermonuclear fusion”, *Nucl. Fusion* **17** 1 (1977).
- Ref7. M. H. SIKORA AND H. R. WELLER, “A New Evaluation of the $^{11}\text{B}(p,\alpha)\alpha$ Reaction Rates”, *J. Fusion Energy* **35** 538 (2016).
- Ref8. S. V. PUTVINSKI et al., “Fusion reactivity of the pB¹¹ plasma revisited”, *Nucl. Fusion* **59** 076018 (2019).
- Ref9. T. WATANABE et al., “Ignition Condition for p-11B Reactor with LHD type Magnetic Field Configuration”, *J. Plasma Fusion Res. SERIES* **6** 630 (2004).

- Ref10. Y. TAKEIRI et al., “High Performance of Neutral Beam Injectors for Extension of LHD Operational Regime”, *Fusion Sci. Technol.* **58** 482 (2010).
- Ref11. F. NESPOLI et al., “First impurity powder injection experiments in LHD”, *Nucl. Mater. Energy* **25** 100842 (2020).
- Ref12. S. MURAKAMI et al., “Finite β Effects on the ICRF and NBI Heating in the Large Helical Device”, *Trans. Fusion Technol.* **27** 256 (1995).
- Ref13. P. VINCENZI et al., “Upgrades and application of FIT3D NBI-plasma interaction code in view of LHD deuterium campaigns”, *Plasma Phys. Control Fusion* **58** 125008 (2016).
- Ref14. K. OGAWA et al., “Time dependent neutron emission rate analysis for neutral-beam-heated deuterium plasmas in a helical system and tokamaks”, *Plasma Phys. Control Fusion* **60** 095010 (2018).
- Ref15. S. P. HIRSHMAN and O. BETANCOURT, “Preconditioned descent algorithm for rapid calculations of magnetohydrodynamic equilibria”, *J. Comput. Phys.* **96** 99 (1991).
- Ref16. S. SUZUKI et al., “Attenuation of high-energy neutral hydrogen beams in high-density plasmas”, *Plasma Phys. Control. Fusion* **40** 2097 (1998).
- Ref17. M. ISOBE et al., “Lorentz Alpha Orbit Calculation in Search of Position Suitable for Escaping Alpha Particle Diagnostics in ITER”, *J. Plasma Fusion Res. SERIES* **8** 330 (2009).
- Ref18. T. IDO et al., “Development of 6-MeV Heavy Ion Beam Probe on LHD”, *Fusion Sci. Technol.* **58** 436 (2010).
- Ref19. M. YOSHINUMA et al., “Charge-Exchange Spectroscopy with Pitch-Controlled Double-Slit Fiber Bundle on LHD”, *Fusion Sci. Technol.* **58** 375 (2010).

- Ref20. T. AKIYAMA et al., “Interferometer Systems on LHD”, *Fusion Sci. Technol.* **58** 352 (2010).
- Ref21. I. YAMADA et al., “Recent Progress of the LHD Thomson Scattering System”, *Fusion Sci. Technol.* **58** 345 (2010).
- Ref22. H. RYUFUKU, “PARTIAL CROSS SECTIONS FOR CHARGE TRANSFER. IN COLLISIONS OF MULTICHARGED IONS. WITH ATOMIC HYDROGEN”, *JAERI-M* 82-031 (1982).
- Ref23. K. OGAWA et al., “Study of first orbit losses of 1 MeV tritons using the Lorentz orbit code in the LHD”, *Plasma Sci. Technol.* **21** 025102 (2018).
- Ref24. M. TOKITANI et al., “Plasma wall interaction in long-pulse helium discharge in LHD – Microscopic modification of the wall surface and its impact on particle balance and impurity generation”, *J. Nucl. Mater.* **463** 91 (2015).
- Ref25. M. TOKITANI et al., “Initial growth phase of W-fuzz formation in ultra-long pulse helium discharge in LHD”, *Nucl. Mater. Energy* **12** 1358 (2017).
- Ref26. K. OGAWA et al., “Installation of Bidirectional Lost Fast-Ion Probe in the Large Helical Device”, *J. Plasma Fusion Res. SERIES* **8** 655 (2009).
- Ref27. G. MARTIN et al., “15 MeV Proton Emission from JET Plasmas Exhibiting Sawtooth Behaviour: Results and Interpretation”, *Phys. Scr.* **T16** 171 (1987).
- Ref28. A. V. KRASILNIKOV et al., “Tokamak Fusion Test Reactor charge exchange atom spectrometry using a natural diamond detector”, *Rev. Sci. Instrum.* **70** 1107 (1999).
- Ref29. S. HIROKI AND M. WATANABE, “Radiation-hardened configuration context realization for field programmable gate arrays”, *Appl. Opt.* **59** 5680 (2020).
- Ref30. P. A. JEGGO, L. H. Pearl, and A. M. Carr, “DNA repair, genome stability and cancer: a historical perspective”, *Nat. Rev. Cancer* **16** 35 (2016).

ACKNOWLEDGEMENT

We acknowledge TAE Technologies for discussing the p-¹¹B fusion estimation in an LHD.

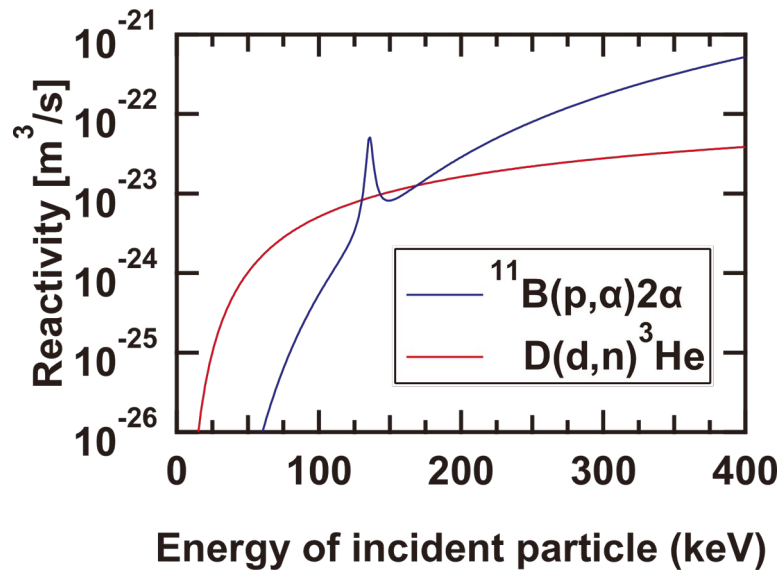


Figure 1. Reactivity of the $^{11}\text{B}(p,\alpha)2\alpha$ reaction as a function of incident particle energy. The reactivity of $\text{D}(d,n)^3\text{He}$ is also shown for comparison.

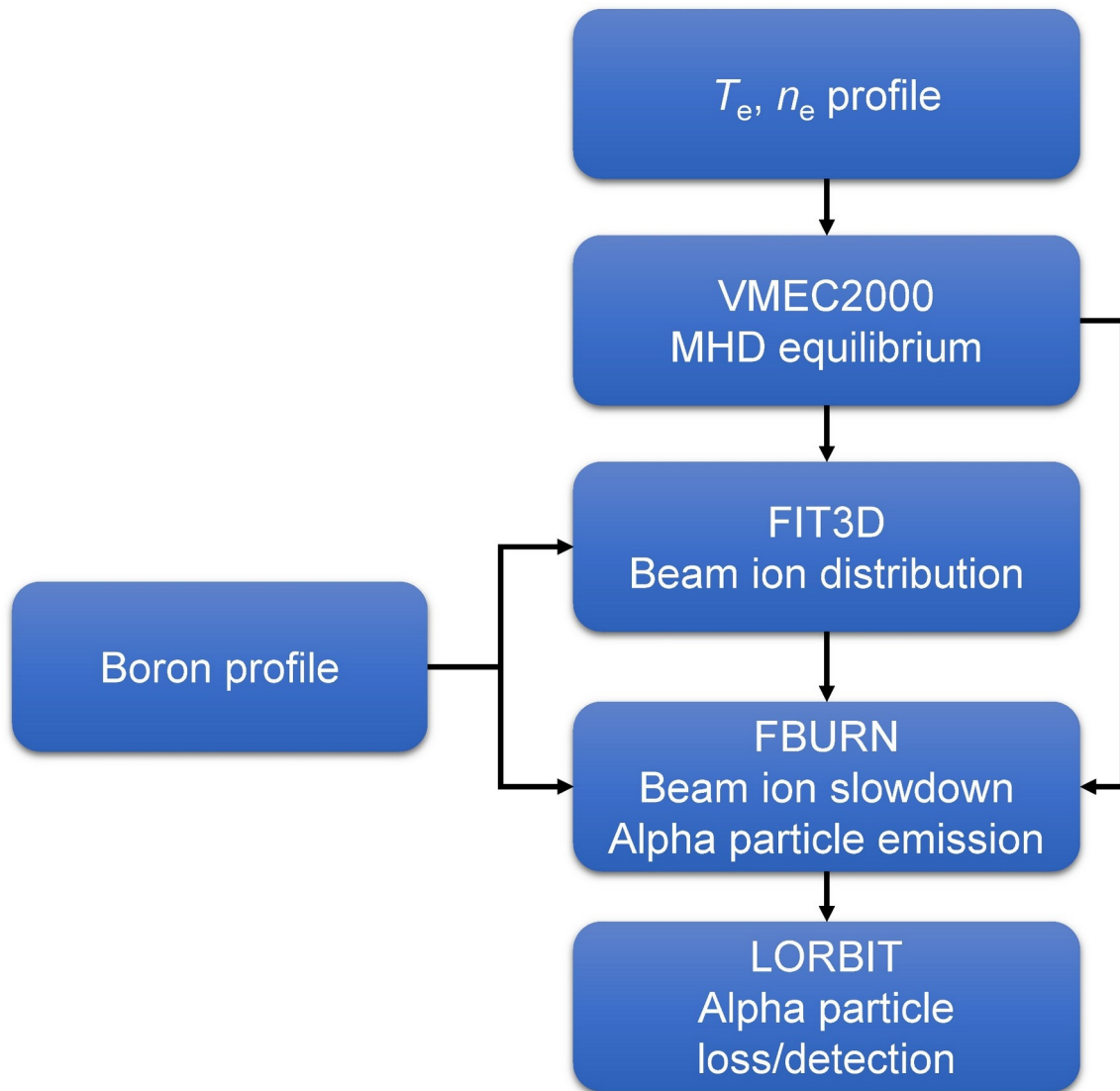


Figure 2 Calculation scheme to evaluate the α particle emission rate.

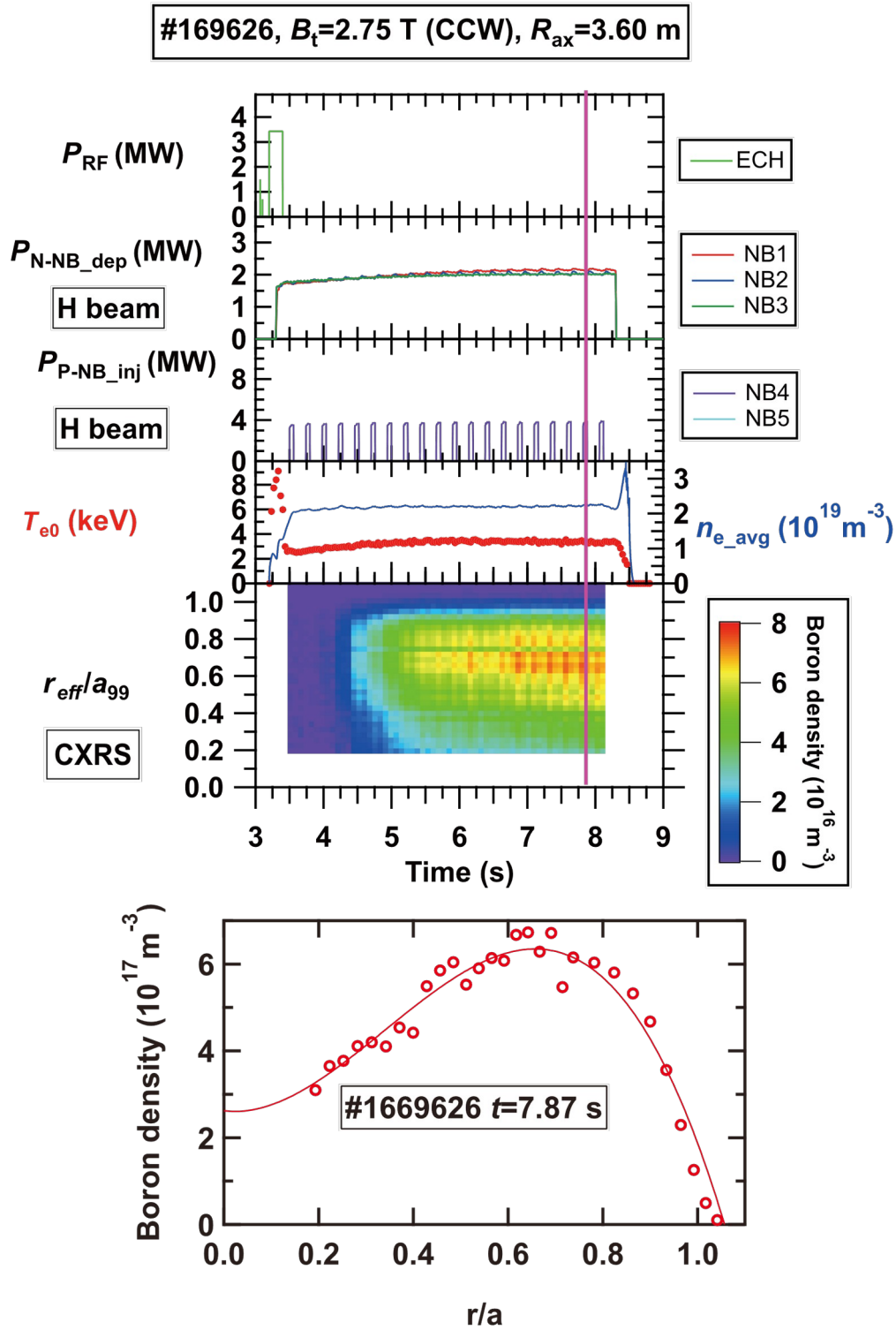


Figure 3 (top) Typical waveforms of boron drop discharge. (bottom) The radial profile of boron density measured by CXRS at $t = 7.87$ s.

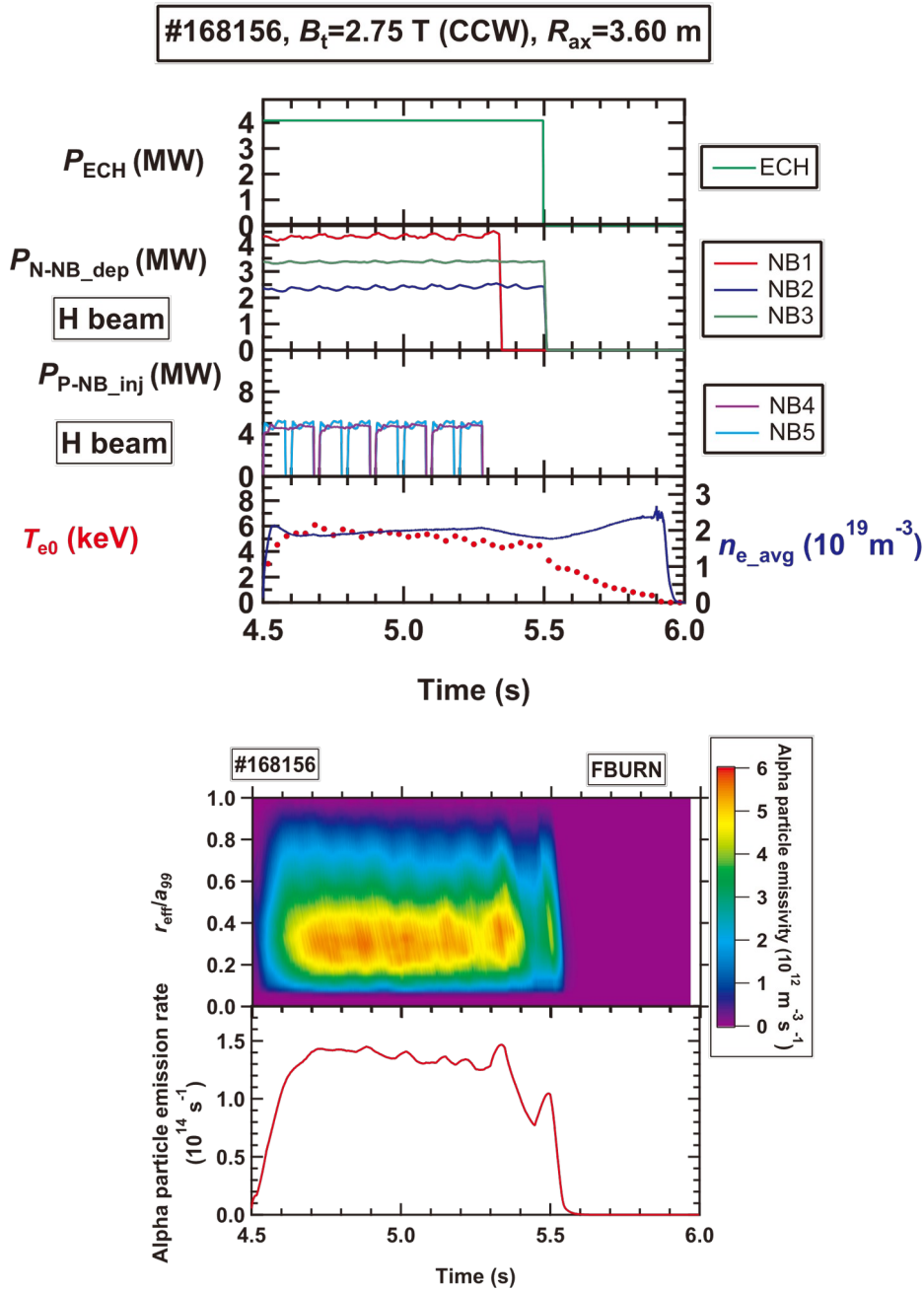
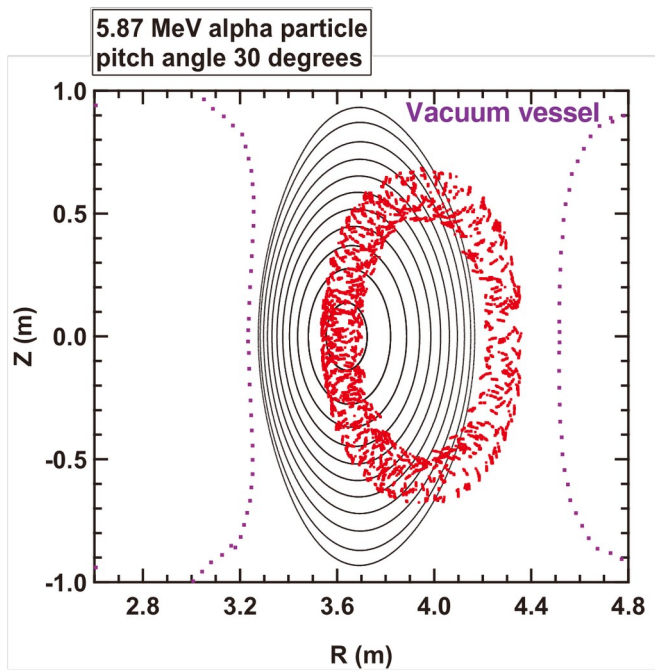


Figure 4 (top) Typical waveforms of hydrogen discharge in LHD. Injection power of NB reaches more than 9 MW for N-NBs and more than 8 MW for P-NBs. (bottom) Time evolution of radial profile of alpha particle emissivity and time evolution of the alpha particle emission rate calculated by the FBURN code. The radial profile of alpha particle emissivity has a peak around r_{eff}/a_{99} of 0.3.

Vertically elongated poloidal cross section



Horizontally elongated poloidal cross section

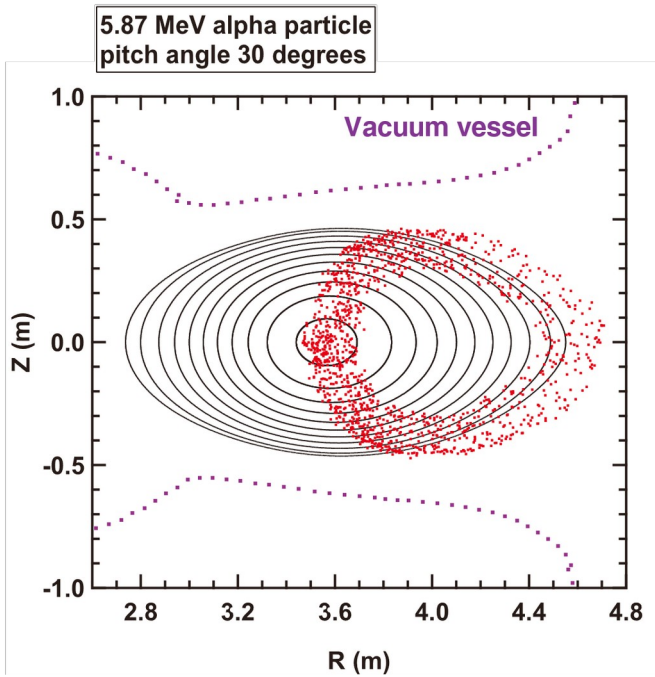


Figure 5 Typical Poincaré plots of the α particle orbit in (top) vertically elongated and (bottom) horizontally elongated cross sections.

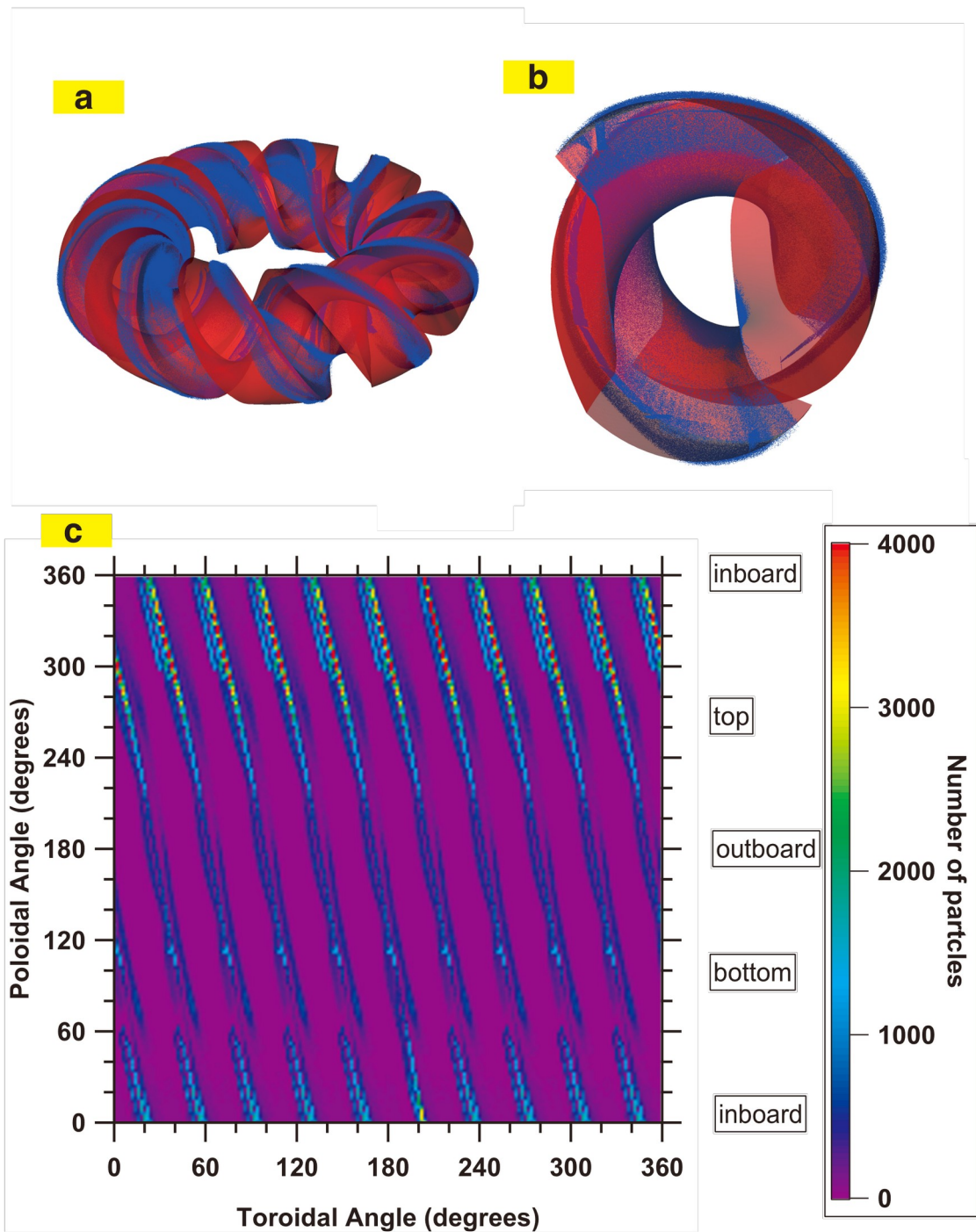


Figure 6 (a, b) Three-dimensional distribution of α particle loss on the vacuum vessel and the divertor plate. (c) Toroidal/poloidal distribution of α particle loss on the vacuum vessel and the divertor plate.

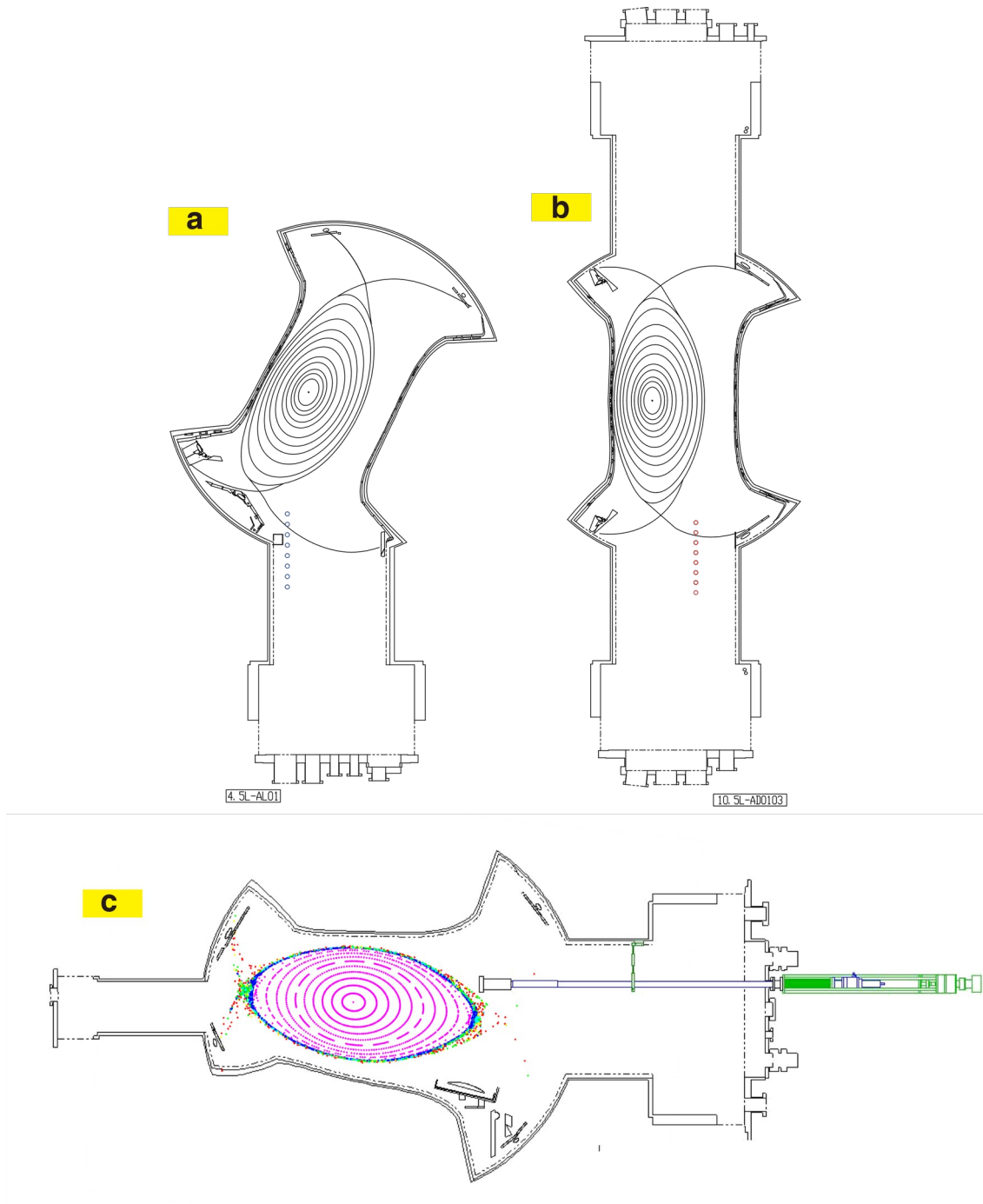


Figure 7 Poloidal cross sections of plasma at (a) the 4.5 L manipulator, (b) the 10.5 L manipulator, and (c) the FILD positions.

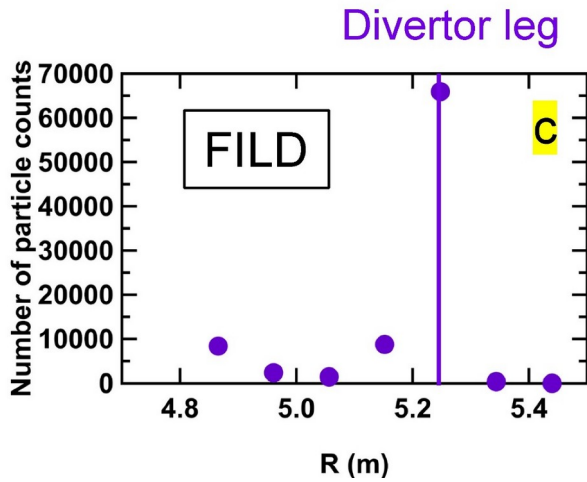
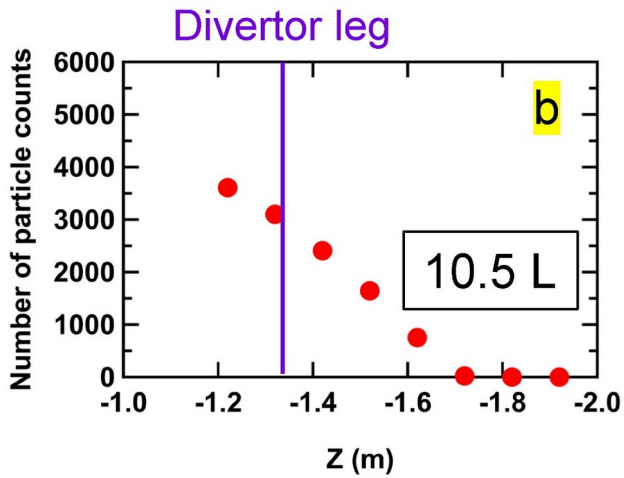
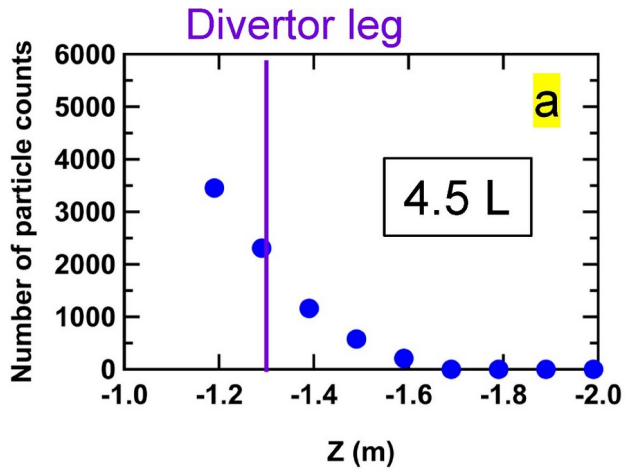


Figure 8 Numbers of alpha particles reaching (a) the 4.5 L manipulator, (b) the 10.5 L manipulator, and (c) the FILD.

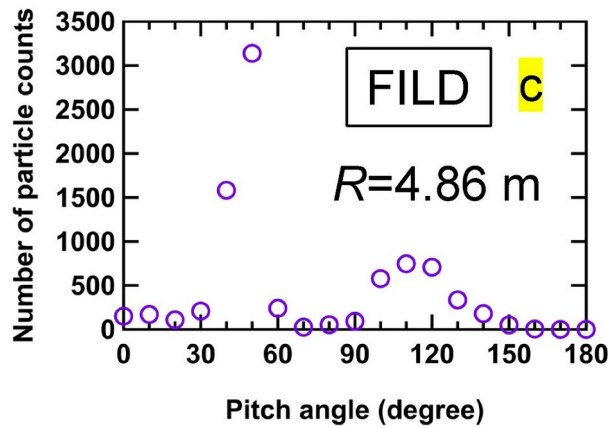
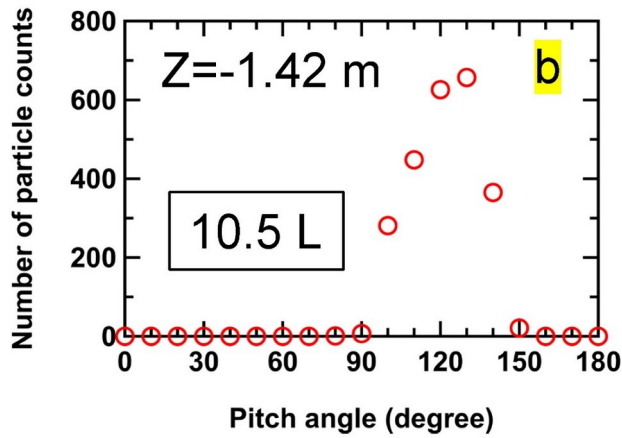
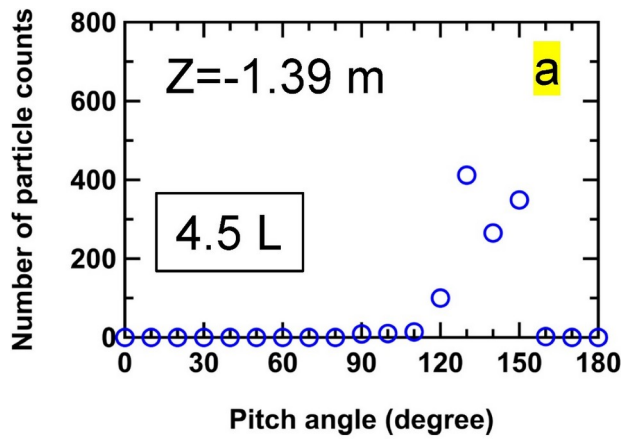


Figure 9 Pitch angle distributions of alpha particles reaching (a) the 4.5 L manipulator, (b) the 10.5 L manipulator, and (c) the FILD.